Simulation of a turbulent annulus with interfacial waves in core-annular pipe flow

Li, Haoyu; Pourquié, M. J.B.M.; Ooms, G.; Henkes, R. A.W.M.

DOI
10.1016/j.ijmultiphaseflow.2022.104152

Publication date
2022

Document Version
Final published version

Published in
International Journal of Multiphase Flow

International Journal of Multiphase Flow 154 (2022) 104152

Contents lists available at ScienceDirect

International Journal of Multiphase Flow

journal homepage: www.elsevier.com/locate/ijmulflow

Simulation of a turbulent annulus with interfacial waves in core-annular pipe flow

Haoyu Li *, M.J.B.M. Pourquié, G. Ooms, R.A.W.M. Henkes

Delft University of Technology, The Netherlands

ARTICLE INFO

Keywords:
Core-annular flow
interfacial waves
friction factor
hold-up ratio

ABSTRACT

Interfacial waves in core-annular pipe flow are studied through two-phase numerical simulations. Here the water annulus is turbulent, whereas the oil core stays laminar. The low-Reynolds number Launder & Sharma $k-\varepsilon$ model is applied. By extracting the moving wave shape from the two-phase results and imposing this as a solid boundary in a single-phase simulation for the water annulus gives single-phase results (for the pressure drop and holdup ratio) that are in close agreement with values obtained from the two-phase approach. The influence of wave amplitude and wave length on the pressure drop and hold up ratio is then studied by using the single-phase flow model. This gives insight in the appearance of core-annular flow, where the water-based Fanning wall-friction factor and the hold-up ratio are selected as the most important quantities. The effect of watercut and eccentricity on these quantities is also investigated.

1. Introduction

Core-annular flow is a typical flow regime for liquid-liquid transport in a pipeline. The flow consists of a viscous core liquid (e.g. oil) and a far less viscous annulus liquid (e.g. water). The water lubrication causes that the pressure drop required to transport viscous oil is much less than what is needed for single-phase viscous oil transport. Over the past decades an extensive literature on core-annular flow has appeared. This is because of its industrial applications and its richness of fluid mechanics fundamentals (see e.g. Joseph et al., 1997, and Ghosh et al., 2009).

Due to the apparent slip effect between the two phases, interfacial waves will be formed. For a laminar water annulus, the dominant wave length can be predicted with stability theory (Chen et al. (1990), Bai et al. (1992)). Some experimental studies (like Rodriguez & Bannwart (2006), Tripathi et al. (2017)) succeeded in measuring the interfacial wave characteristics (incl. wave amplitude, wave length, and wave speed). The appearance of interfacial waves will make the flow characteristics (like pressure drop and holdup ratio), for given liquid-liquid flow rates, different from those found with a flat liquid-liquid interface (so-called Perfect Core-Annular flow). Bannwart (2001) and Ullmann & Brauner (2004) developed semi-empirical two-fluid models to predict the pressure drop and hold up ratio. The wall friction factor and the interfacial friction factor appear in the two-fluid model, and empirical correlations are used for closure. A good understanding of liquid-liquid interaction at the interface is thus important for core-annular flow modelling.

Most studies have considered a laminar annulus flow, but the present study will focus on core-annular flow with a turbulent annulus. The simulation of such flow is quite challenging because of the presence of both the turbulent water annulus and the interface with travelling waves. The interface capturing method (e.g. Volume of Fluid, Level Set method) has been applied in various studies, e.g. Ingen Housz et al. (2017) and Kim & Choi (2018). A very fine mesh, with large computational effort, is needed to obtain a sharp and accurate interface. Bai et al. (1996) assumed a sharp interface, and they simulated the 2D wave shape by iterating the force balance across the interface; the converged wave shape compared quite well with experiments. In oil-water core-annular flow, the ratio of the oil and water viscosities is very high, causing that the oil core moves approximately as a solid body with a fixed wave pattern. Ooms et al. (2012) adopted the 2D wave shape from the results by Bai et al. (1996) in 3D eccentric simulations with a laminar water annulus. By assuming the oil core to behave as a solid body, a downward levitation force is found on the oil core at higher Reynolds numbers.

The present study builds on our previous work on core-annular flow (Li et al. 2021). Turbulence in the water annulus is represented by using the RANS approach (Reynolds-Averaged Navier-Stokes), applying the $k-\varepsilon$ model with the Launder-Sharma low-Reynolds number terms. A number of other studies have followed a similar approach (either with

* Corresponding author:
E-mail address: h.li-6@tudelft.nl (H. Li).

https://doi.org/10.1016/j.ijmultiphaseflow.2022.104152
Received 10 February 2022; Received in revised form 19 May 2022; Accepted 1 June 2022
Available online 2 June 2022

variants of the $k-\varepsilon$ model or the $k-\omega$ model; see Huang et al. (1994), Ko et al. (2002), Ingen Housz et al. (2017). Despite shortcomings with RANS in modelling the complex water annulus flow, particularly due to the presence of a wavy interface, it can still be an attractive way of studying flow structures as a function of the many parameters that play a role in core annular flow, such as: watercut, Reynolds number, viscosity ratio, density ratio, pipe inclination, liquid-liquid interfacial tension.

A number of studies was devoted to pressure drop and holdup for core annular flow, either through experiments or through theoretical models and simulations. These studies include: Arney et al. (1993), Shi et al. (2017), Hu et al. (2020); these inspired us to focus our study on the behaviour of the dimensionless pressure drop relation and the holdup relation in core-annular flow. For the dimensionless pressure drop, the water-based Fanning friction factor will be used. This can answer how the pressure drop for core-annular flow compares to the case in which only water is flowing through the pipe. For the holdup, the so-called holdup ratio will be used. This describes the relative water accumulation compared to the watercut (which is an indicator of relative slip between two liquid phases). As a first estimate, the wall friction factor for core-annular flow can be taken equal to the value for water-only flow (at the same flow rate as the corresponding combined water-oil flow rate for core-annular flow). But the presence of the viscous core will have an effect on the turbulence in the water annulus, which might thus be different from the turbulence found for single-phase water flow. The formation of waves at the interface will decrease the total water accumulation giving a smaller average thickness of the water annulus. This gives a higher average bulk water velocity, which increases the wall friction (and herewith the pressure drop and friction factor). But the larger oil core and thinner average water annulus may also hinder the turbulence in the annulus, which will tend to decrease the wall friction. What is the final balance for core-annular flow, i.e. between oil and water flow rates on one hand versus pressure drop and hold-up on the other hand?

To answer this, 2D two-phase simulations were performed for different conditions. In addition also 2D and 3D single-phase simulations were carried out for only the water annulus, with imposed waves (with varying wave length and wave amplitude) at the location of the two-phase interface. In this way the effect of the wavy interface on the friction factor and holdup ratio could be systematically assessed. In particular also the effect of watercut and core eccentricity was simulated.

2. Modelling approach

2.1. Governing equations

The mass and momentum conservation equations for an incompressible, isothermal fluid are (in Cartesian coordinates):

$$\frac{\partial u_i}{\partial x_i} = 0 \tag{1}$$

$$\frac{\partial \rho u_i}{\partial t} + \rho u_j \frac{\partial u_i}{\partial x_j} = \frac{\partial}{\partial x_j}\left(\rho(\nu+\nu_t)\left(\frac{\partial u_i}{\partial x_j}+\frac{\partial u_j}{\partial x_i}\right)\right) - \frac{\partial p}{\partial x_i} + \rho g_i + F_{\sigma,i} \tag{2}$$

These are the Reynolds-Averaged Navier-Stokes Equations (RANS). Here u_i is the velocity, ρ and μ are the fluid density and viscosity, g_i is gravitational acceleration, p is pressure and $F_{\sigma,i}$ is the interfacial tension force. For pipe flow, we will use $x_1 = x$ for the coordinate along the horizontal pipe axis, $x_2 = y$ for the vertical coordinate, and $x_3 = z$ for the pipe width coordinate; the velocity components are u, v, and w, in directions x, y, and z, respectively. The gravity components are: g_1=g_3=0, and $g_2 = -g$, where g is gravitational acceleration.

The turbulent viscosity is modelled with the low-Reynolds number $k-\varepsilon$ model of Launder & Sharma (1974), which reads as follows:

$$\nu_t = C_\mu f_\mu \frac{k^2}{\widetilde{\varepsilon}} \tag{3}$$

$$\frac{\partial k}{\partial t} + u_j \frac{\partial k}{\partial x_j} = \frac{\partial}{\partial x_j}\left(\nu + \frac{\nu_t}{\sigma_k}\right)\frac{\partial k}{\partial x_j} + \nu_t\left(\frac{\partial u_j}{\partial x_j}\right)^2 - \widetilde{\varepsilon} - D \tag{4}$$

$$\frac{\partial \widetilde{\varepsilon}}{\partial t} + u_j \frac{\partial \widetilde{\varepsilon}}{\partial x_j} = \frac{\partial}{\partial x_j}\left(\nu + \frac{\nu_t}{\sigma_\varepsilon}\right)\frac{\partial \widetilde{\varepsilon}}{\partial x_j} + C_1 f_1 \frac{\widetilde{\varepsilon}}{k}\nu_t\left(\frac{\partial u_j}{\partial x_j}\right)^2 - C_2 f_2 \frac{\widetilde{\varepsilon}^2}{k} + E \tag{5}$$

With $D = 2\nu\frac{\partial\sqrt{k}}{\partial x_j}\frac{\partial\sqrt{k}}{\partial x_j}$ and $E = 2\nu\nu_t\left(\frac{\partial^2 u_j}{\partial x_j^2}\right)^2$. The turbulent energy dissipation rate is $\varepsilon = \widetilde{\varepsilon} + D$. Furthermore, $C_\mu = 0.09$, C_1=1.44, C_2=1.92, σ_k=1.0, σ_ε=1.3, $f_\mu = \exp\left(\frac{-3.4}{\left(1+\frac{Re_t}{50}\right)^2}\right)$, f_1=1, $f_2 = 1 - 0.3\exp(-Re_t^2)$, $Re_t = \frac{k^2}{\varepsilon\nu}$. Boundary conditions at the wall are: k=0 and $\bar{\varepsilon} = 0$.

Quite a number of low-Reynolds number $k-\varepsilon$ formulations are available in the literature. A large advantage of the Launder-Sharma one is that the low-Reynolds number terms do not include the explicit distance to the closest wall. Instead the parameter Re_t is used to incorporate the effect of turbulence damping when a wall is approached. In the same way, the model incorporates possible damping of turbulence when the oil-water interface is approached in core-annular flow. The low-Reynolds number $k-\varepsilon$ model is used everywhere in the domain, also in the laminar oil core. Because of the presence of the low-Reynolds number terms the model automatically relaminarizes in the viscous oil core (i.e. it gives zero turbulent viscosity).

2.2. Numerical method

We used the open-source package OpenFOAM to solve the RANS equations, applying the CLSVOF method for interface capturing. The CLSVOF solver, which was developed by Yamamoto et al. (2017), is based on the interFoam Volume of Fluid (VOF) solver in OpenFOAM. The level set function was used to calculate the interfacial tension force. Starting from the VOF method, the oil volume fraction α is introduced to distinguish between two fluid phases: $\alpha = 0$ is the oil phase, $\alpha = 1$ is the water phase, and $0 < \alpha < 1$ denotes the oil-water interface. Then the fluid density and viscosity in the equations are:

$$\rho = (1-\alpha)\rho_o + \alpha\rho_w \tag{6}$$

$$\mu = (1-\alpha)\mu_o + \alpha\mu_w \tag{7}$$

The subscript "o" refers to oil, and the subscript "w" refers to water. α is calculated from the following advection equation:

$$\frac{\partial \alpha}{\partial t} + \nabla\cdot(\alpha\vec{u}) + \nabla\cdot\left((1-\alpha)\alpha\vec{u}_r\right) = 0 \tag{8}$$

The third term on the left-hand side is the compressive term (with the divergence of the compressive flux); here $\vec{u}_r = \vec{u}_w - \vec{u}_o$. This term is meant to control the sharpness of interface.

The level set function Φ is defined as the distance from the interface, where the interface is the isoline with $\Phi = 0$. The initial value of the level set function Φ_o is obtained from the initialized volume-of-fluid field, where the interface is defined at $\alpha = 0.5$:

$$\Phi_0 = (2\alpha - 1)\Gamma \tag{9}$$

$$\Gamma = 0.75\Delta X \tag{10}$$

Here ΔX is the minimum mesh size near the interface. Thereafter the re-initialization equation is solved to turn the initial level set function into the distance from the interface:

$$\frac{\partial \Phi}{\partial \tau} = \mathrm{sign}(\Phi_0)(1 - |\nabla\Phi|) \tag{11}$$

Here $\tau = 0.1\Delta X$ is the iteration time step of Φ and the sign function

denotes:

$$\text{sign}(\Phi) = \begin{cases} 1 & \Phi > 0,\ water \\ 0 & \Phi = 0,\ interface \\ -1 & \Phi < 0,\ oil \end{cases} \tag{12}$$

Then the interface tension force is calculated as:

$$\vec{F}_\sigma = \sigma\kappa(\Phi)\delta_\Phi \nabla(\Phi) \tag{13}$$

Here σ is the interface tension and δ_Φ is the smoothed delta function:

$$\delta_\Phi = \begin{cases} \frac{1}{2\gamma}\left(1+\cos\left(\frac{\pi\Phi}{\gamma}\right)\right) & for\ |\Phi| < \varepsilon \\ 0 & elsewhere \end{cases} \tag{14}$$

The quantity γ is the interface thickness coefficient (see Yamamoto et al., 2017) and $\kappa(\Phi)$ is the interface curvature:

$$\kappa(\Phi) = \nabla \cdot \vec{n}_c \tag{15}$$

$$\vec{n}_c = \frac{(\nabla\Phi)_f}{\left|(\nabla\Phi)_f\right|} \tag{16}$$

Here $\vec{n}_c$ is the surface unit normal vector. The contact angle θ between interface and pipe wall is defined as:

$$\cos(\theta) = \vec{n}_c \cdot \vec{n}_w \tag{17}$$

With $\vec{n}_w$ being the unit normal vector at the wall. The contact angle is set to 90^o in our simulations. This means that both the level set function Φ and the volume fraction of the fluid α satisfy the zero gradient condition at the pipe wall boundary.

A pressure drop in flow direction is added as an extra force term to the right-hand side of equation (2), with periodic boundary conditions on the left and right side of the pipe. Therefore, the pressure that remains in the equations is periodic with respect to the left and right side of the computational pipe section. The initially assumed velocity profile will then develop over time under this pressure drop in the transient simulation until a stable state is obtained.

A second-order backward implicit time discretization scheme is applied, with a very small time step (small Courant number). This gives a very accurate time integration. We use a second-order scheme for advection terms in the momentum equations and in the interface equation (as used in the level set method), but a first-order upwind scheme for advection in the equations for the turbulence quantities k and ε; trying a second-order scheme for the latter gave numerical instabilities. Through successive mesh refinement, however, we have verified that the simulation results are accurate (and not suffering from large numerical diffusion).

In all the simulations, periodic boundary conditions are applied on the left and right side of the pipe, which restricts the wavelengths in the axial direction to the domain length divided by an integer value. At the pipe wall, the no-slip condition is imposed. We have used the symmetric PBiCG solver for velocity and for turbulent quantities, the GAMG solver for pressure, and the PIMPLE solver for velocity-pressure coupling.

2.3. Basic simulation set-up

In the simulations for the basic set-up, the following parameters were kept the same as in the experiments carried out in our lab. The pipe radius is R=0.0105 m (pipe diameter is 21 mm). The length of the pipe section was set to 0.0256 m (25.6 mm), which is twice the most dominant wavelength, as estimated from a linear instability analysis (albeit for laminar flow) by Beerens et al. (2014). The section length was also varied to investigate its effect on wave selection. The fluid properties were set as follows: oil and water kinematic viscosity are $\nu_o = 7.73\times10^{-4}$ m^2/s and $\nu_w = 6.7\times10^{-7}$ m^2/s, the oil and water densities are $\rho_o = 902$ kg/m^3 and $\rho_w = 993$ kg/m^3, and interfacial tension between oil and water is $\sigma = 0.016$ N/m (Shell Morlina S2 B 680 at 40 °C was used in the experiments). Note that the ratio between kinematic viscosities of oil and water is 1150, and the density ratio between oil and water is $\rho_o/\rho_w = 0.91$. The Reynolds number in wall units, i.e. $Re_\tau = d^+ = u_\tau d/\nu_w$, is about 150 (here u_τ is the wall shear stress velocity and d is the average thickness of the water annulus). This is above the minimum value of about 90 which is needed to sustain turbulence in single-phase channel flow (where d is half the channel width); this criterion was derived by Jiménez & Moin (1991), who applied DNS (Direct Numerical Simulations) to channel flow. The occurrence of turbulence in the water annulus is confirmed in the present simulations, which shows an inertial sublayer with a maximum turbulent viscosity (ν_t/ν_w) of about 20.

2.4. Key parameters

Four important parameters are: total flow rate, pressure drop, watercut, and water holdup fraction. When two parameters are set as input (e.g. total flow rate and watercut in the experiments), the other two will follow as output.

The watercut is defined as the ratio of water volumetric flow rate and total volumetric flowrate:

$$\text{WC} = Q_w/(Q_o + Q_w) \tag{18}$$

where Q denotes the volumetric flow rate. The water holdup fraction is defined as the ratio of the in-situ water volume in the pipe and the total volume of oil and water:

$$\alpha_w = \frac{V_w}{V_w + V_o} \tag{19}$$

A related parameter is the so-called holdup ratio h, which is defined as:

$$h = \frac{Q_o/Q_w}{V_o/V_w} \tag{20}$$

This can also be rewritten as $h = 1 + u_r/u_w$. Here the velocity difference $u_r = u_o - u_w$, is the apparent (average) slip velocity between oil core (having a bulk velocity u_o) and water annulus (having a bulk velocity u_w). Note that h=1 when there is no slip between bulk oil and water velocities. The holdup ratio thus is a measure of apparent slip between oil core and water annulus.

When waves appear at the liquid-liquid interface, the wave amplitude can be defined as

$$A = \sqrt{2\overline{(\delta - \bar{\delta})^2}} \tag{21}$$

Here δ is the instantaneous thickness of the annulus; an overbar denotes the averaged value (in space and time). The amplitude is defined such that it gives the usual value of the amplitude for the case that the wave is a pure sinus (where the amplitude is half the difference between the maximum and the minimum value).

2.5. Force balance

It will be helpful for the interpretation of the results to also consider the integral force balance for the flow (after averaging in space and time), using quantities shown in Figure 1. Here x is the streamwise pipe coordinate, and r is the radial pipe coordinate. The pipe has radius R. Oil flow is represented by a concentric core with radius R_c. Water flows in an annulus with thickness $R - R_c$. The flow is driven by the pressure gradient $-dp/dx$. The wall imposes a wall shear stress τ_W on the water annulus (taken positive in upstream direction). The water annulus imposes an interfacial stress τ_i on the oil core (taken positive in upstream direction). The oil core also imposes an interfacial stress on the water annulus, which has the same magnitude as τ_i, but now taken positive in downstream direction. Water and oil flow with an average velocity (bulk

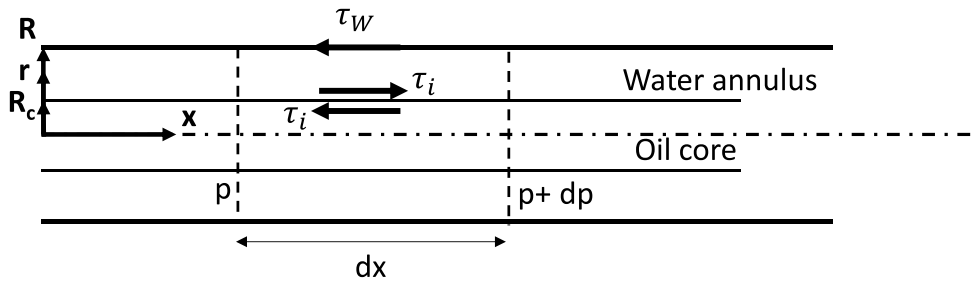

Figure 1. Stresses imposed on core-annular flow

velocity) u_w and u_o, respectively. The bulk velocity follows from the superficial velocity as: $u_w = u_{sw}/\alpha_w$ and $u_o = u_{so}/\alpha_o$, with $u_{sw} = Q_w/A_p$ and $u_{so} = \frac{Q_o}{A_p}$. Here $A_p = \pi R^2$ is the cross sectional area of the pipe.

The force balance for the combined oil-water flow in a horizontal pipe reads:

$$-\frac{dp}{dx}A_p - \tau_W 2\pi R = 0 \tag{22}$$

The force balance for the oil core gives:

$$-\frac{dp}{dx}\alpha_o A_p - \tau_i 2\pi R_c = 0. \tag{23}$$

Here α_o is the oil holdup fraction, with $\alpha_o = (R_c/R)^2$.

From force balances (22) and (23) it also follows that the wall shear stress and interfacial stress are related as $\tau_i = \tau_W R_c/R$. Note that the force balances (22) and (23) hold for core-annular flow (with or without interfacial waves) after averaging in space and time.

Due to the considered high ratio of the oil and water viscosities, the oil core will be laminar. The typical streamwise velocity profile is shown in Figure 2. As the oil viscosity is high, the oil velocity is almost constant throughout the core Assuming parallel flow in the laminar oil core (i.e. neglecting non-parallel effects in the oil flow close to the wave interface), the flow here can be described by the force balance:

$$-\frac{dp}{dx}\pi r^2 - \mu_o \frac{du}{dr}2\pi r = 0, \tag{24}$$

with interface condition: $\tau_i = -\mu_o\left(\frac{du}{dr}\right)_{r=R_c}$.

Integration gives the following expression for the interface velocity:

$$u_i = -\frac{R_c}{4\mu_o}\tau_i + \frac{Q_o}{\pi R_c^2}, \tag{25}$$

in which $Q_o$is the oil flow rate. For all conditions considered in the present study, the first term on the right hand side is much smaller than the second term. This means that within the boundaries of validity of the shown force-balance approach with parallel core flow, the interfacial velocity is the same as the bulk oil velocity.

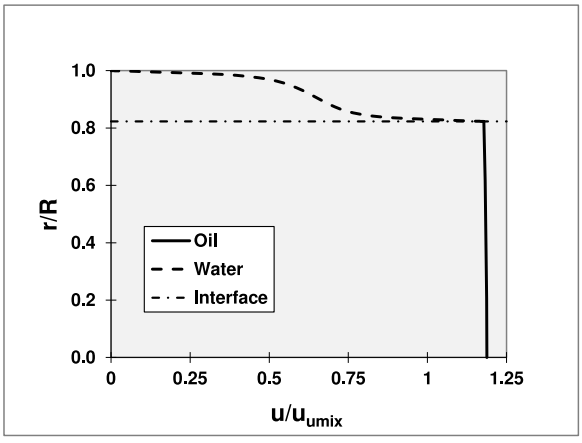

Figure 2. Typical streamwise velocity profile for core-annular flow (the example conditions are set to 20% watercut and an interface without waves).

2.6. Mechanistic models

The force balance method as discussed in the previous subsection can be used to determine a mechanistic model for core-annular flow. The most simple mechanistic modelling approach for core-annular flow is obtained by assuming that the frictional pressure drop (or the wall shear stress) is the same as found for a fully turbulent pipe flow that transports single-phase water, in which the water flow rate is taken the same as the total oil plus water flow rate for the corresponding core-annular flow. This seems to be a rough assumption, but the present study will show that it is in fact quite accurate. The Reynolds number for this flow is based on the water properties and on the mixture velocity. The wall shear stress τ_W in the overall pipe flow balance (22) can be expressed as $\tau_W = f_W \frac{1}{2}\rho_w u_m^2$, in which f_W is the Fanning friction factor. Substitution into eq. (22) gives:

$$f_W = -\frac{dp}{dx}\frac{R}{\rho_w u_m^2} \tag{26}$$

The mixture velocity is defined as $u_m = \frac{Q_w+Q_o}{A}$. Different very accurate correlations exist in the literature to describe the Fanning friction factor for single-phase pipe flow. An accurate example is the Churchill correlation, which reads (for a smooth wall):

$$f_W = 2\left[\left(\frac{8}{Re_w}\right)^{12} + \frac{1}{(A^*+B^*)^{3/2}}\right]^{1/12} \tag{27}$$

$$A^* = \left\{-2.457\ln\left[\left(\frac{7}{Re_w}\right)^{0.9}\right]\right\}^{16} \quad \text{and} \quad B^* = \left(\frac{37530}{Re_w}\right)^{16}$$

The Reynolds number is defined as: $Re_w = \frac{\rho_w D u_m}{\mu_w}$. As an alternative to the Churchill correlation also the Blasius equation can be used: $f_W = \frac{0.046}{Re_w^{0.2}}$.

The Churchill correlation and the Blasius correlation give practically the same values for turbulent single-phase flow; the correlations have been extensively validated against lab experiments and DNS, and are very accurate. Using the single-phase mechanistic modelling approach, the pressure drop for core-annular flow is independent of the water holdup fraction.

Ullmann & Brauner (2004) have proposed a more refined mechanistic model for core-annular flow in horizontal and inclined pipes. They proposed the following empirical expressions for wall shear stress and interfacial stress, as appearing in force balances (22) and (23):

$$\tau_W = \frac{1}{2}\rho_w f_W u_w^2, \text{ with } f_W = C_w \Big/ Re_{sw}^{n_w} \tag{28}$$

$$\tau_i = \frac{1}{2}\rho_o f_i u_o(u_o - C_i u_w), \text{ with } f_i = C_o F_i \Big/ Re_o^{n_o} \tag{29}$$

The Reynolds numbers in these expressions are defined as:

$$Re_{sw} = \frac{\rho_w u_{sw} 2R}{\mu_w} \text{and} Re_o = \frac{\rho_o u_o 2R_i}{\mu_o}$$

Note that the water Reynolds number is based on superficial water velocity and the oil Reynolds number is based on bulk oil velocity. Assuming a turbulent water annulus and a laminar oil core, Ullmann & Brauner use the following values for the different coefficients: $n_w = 0.2$, $C_w = 0.046$, $n_o = 1$, $C_o = 16$, $F_i = 1.0$. The value for C_i can be taken between 1.14 and 1.22; we have used $C_i = 1.17$ in the present study.

After substitution of these correlations, it is straightforward to resolve the pressure drop and holdup ratio from equations (22) and (23). For a high value of the ratio between oil and water viscosities, it turns out that $h = C_i$. We can also relate the pressure drop according to the Ullmann & Brauner model and the single- phase (water-based) model, by rewriting the Ullmann & Brauner expression for the wall shear stress as:

$$\tau_W = f\frac{1}{2}\rho_w u_m^2 \text{ with} f = C^* \frac{0.046}{Re_w^{0.2}} \text{and} C^* = \frac{(1 + WC(h-1))^2}{h^2 WC^{0.2}} \tag{30}$$

WC is the watercut (fraction) and $h = C_i = 1.17$. The Reynolds number is the same as defined for single-phase flow, i.e. $Re_w = \frac{\rho_w D u_m}{\mu_w}$. This shows that the Fanning friction factor is the same as for single-phase water flow (using the Blasius correlation), multiplied by a factor C^* that only depends on the watercut (see Figure 3); it should be noted (according to the authors' knowledge) that the way in which we have rewritten the model has enabled this insightful interpretation, has not been reported in the literature yet. This shows that the friction factor for core-annular flow in the Ullmann & Brauner model only depends on water-based Reynolds number and on watercut. For high watercut, the friction factor follows the single-phase value, whereas for smaller watercut (say below 25%), the friction factor is higher than the single-phase value. Or: for lower watercut the pressure drop for core-annular flow will be higher than what is found with assuming single-phase water flow (with the oil-water mixture velocity).

As described in our previous study (Li et al., 2021), sustaining a fully turbulent water annulus requires that the Reynolds number in wall units (the shear-based Reynolds), i.e. $Re_\tau = d^+ = u_\tau d/\nu_w$, is at least about 90. Here u_τ is the wall shear velocity and d is the average thickness of the water annulus: $u_\tau = \sqrt{\tau_W/\rho_w}$ and $d/D = (1 - \sqrt{1-\alpha_w})/2$. Using the definition of the Fanning friction factor f_W and of the holdup ratio h it follows that:

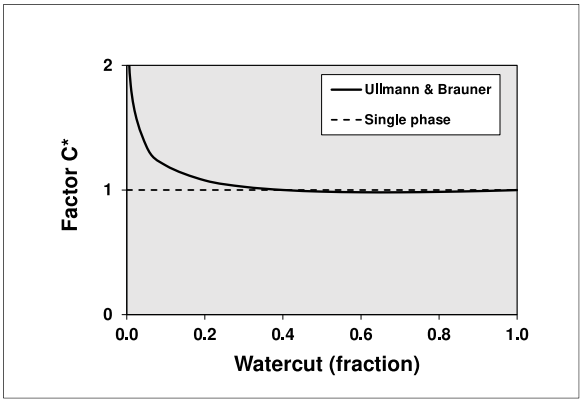

Figure 3. Ratio (=C^*) between the pressure drop according to the Ullmann & Brauner model and single-phase water flow.

$$Re_\tau = \sqrt{\frac{f_W}{8}}\left(1 - \sqrt{\frac{1 - WC}{1 - WC + h\,WC}}\right) Re_W \tag{31}$$

Here WC is the watercut (fraction).

3. Pressure drop in various experiments

To better understand the structure of core-annular flow, we have reviewed different sets of experimental lab data as available in the literature. Relevant parameters as used in these studies are summarized in Table 1. All these experiments are for a horizontal pipe, except for the study by Vanegas Prada (1999), which was for a vertical pipe. But the density difference between oil and water in the latter study is so low that the gravity effect can be neglected, and the results can be compared with those obtained in a horizontal pipe with negligible eccentricity. The considered experiments cover a pipe diameter range between 15.5 and 50 mm, an oil to water viscosity ratio range between 750 and 18000, a density difference range between 20 and 115 kg/m^3, and a value for the water-based Reynolds number Re_w up to 146000. The experiments also cover a range of watercuts.

The measured values of the pressure drop are converted into a Fanning friction factor by using eq. (26). Figure 4 shows the ratio of the Fanning friction factors for the different sets of experiments. That ratio is either the experimental Fanning friction factor divided by the Fanning friction factor for single-phase water flow (using oil-water mixture velocity; see eq. (27)) or the experimental Fanning friction factor divided by Ullmann & Brauner Fanning friction factor (see eq. (30)). The comparison shows that in general the experimental value of the Fanning friction factor (or the pressure drop) is (slightly) higher than the single-phase value. Using the Ullmann & Brauner model gives better agreement with experiments than the single-phase approach. This improvement is fully due to the correction factor (see Figure 3) for the watercut. The improvement is particularly noticeable for the experiments by Oliemans et al. (1987).

All considered experiments have the tendency to give a wall friction factor that is somewhat above the wall friction factor for single-phase water flow. The experiments by Grassi et al. (2008) and by Sotgia et al. (2008) give a wall friction factor that is almost the same as the value for single-phase water flow. This supports that the Fanning wall friction factor is an attractive quantity for the scaling of the pressure drop as measured in different core-annular flow configurations.

Next to the pressure drop, another quantity of interest is the relative water accumulation as expressed by the holdup ratio h. The asymptotic value is $h = 1$ (i.e. no apparent slip between the oil core and the water annulus). The Ullmann & Brauner model applies $h = 1.17$. Bai et al. (1992) proposed $h = 1.39$, as derived from video recordings of their lab experiments. Oliemans (1986) derived the following expression for the holdup ratio as based on photos of the accumulation: $h = 1 + \frac{0.2(1-WC)^4}{1-0.2WC(1-WC)^4}$. Here WC is the watercut (fraction). The value for h in this expression varies from 1.2 for small watercut to 1 for higher watercut.

The experiments mentioned above were taken for a range of watercuts. By determining the shear based-Reynolds number with eq. (31) for all these experiments (using the watercut, the measured pressure drop, and an estimated holdup ratio $h = 1.39$) it is found that the measurements with a watercut of about 15% or lower have a water annulus that is expected to be laminar or not fully turbulent as Re_τ is below 90. The measurements for a watercut of 20% or higher give an annulus that is expected to be in the fully turbulent regime. As an example, Figure 5 shows Re_τ as function of watercut for the experiments by Sotgia et al. (2008) and by Van Duin et al. (2019).

Summary of findings in this section:

- A review of different sets of lab data for core-annular flow shows that the Fanning friction factor for the wall, which makes the pressure

Table 1
Overview of some core-annular flow experiments.

Experiment	Pipe diameter mm	Kin. viscosity ratio	Density diff. kg/m^3	max. Re_w
Oliemans et al. (1987)	50	3000	20	146000
Vanegas Prada (1999)	27.5	18000	35	60000
Grassi et al. (2008)	21	700	115	38000
Sotgia et al. (2008)	26	1000	110	46000
Tripathi et al. (2017)	15.5	100	10	21000
Van Duin et al. (2019)	21	750 - 3000	90	25000

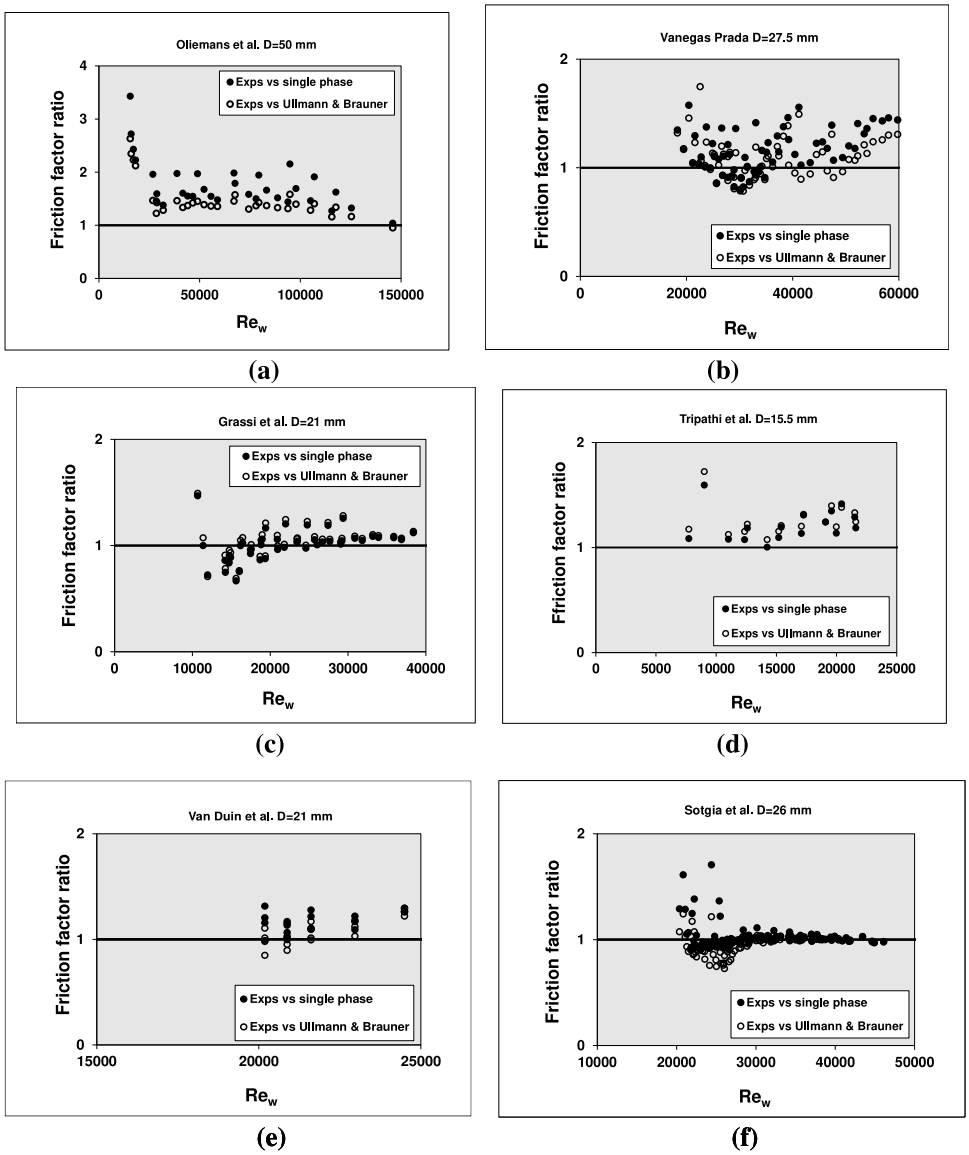

Figure 4. Overview of experimental results for the wall friction factor; experiments by (a) Oliemans et al., (b) Vanegas Prada, (c) Grassi et al., (d) Triphati et al., (e) Van Duin et al., (f) Sotgia et al.

drop dimensionless with the dynamic pressure based on the water density and on the mixture velocity, is an attractive parameter.
- In the experiments, that friction factor is close to the value found for turbulent water-only flow, and almost independent of watercut.

4. Effect of pipe section length

Simulations were carried out with the 2D axisymmetric model for the base case conditions (i.e. with 21 mm diameter, see section 2.3) to determine the dependence of the dominant wave length on the chosen

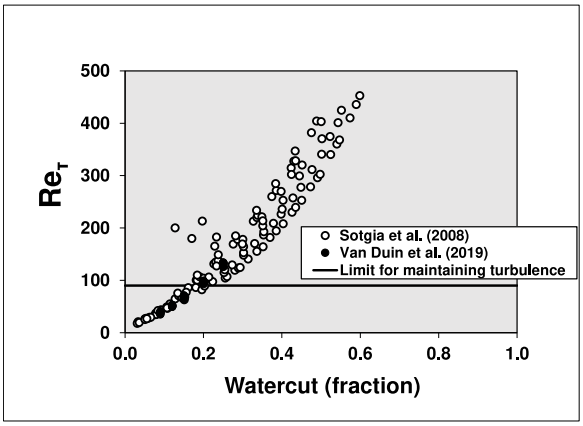

Figure 5. Shear-based Reynolds for different watercuts for which core-annular flow experiments are available.

computational domain in streamwise direction. The imposed total flow rate is 0.00043 m^3/s (i.e. 1.24 m/s mixture velocity) and the imposed water holdup fraction is 0.2573. Periodic boundary conditions are imposed at the inlet and outlet of the section. A simulation example of the wave train is shown in Figure 6. Results for the dominant wave length, and its frequency, amplitude and velocity are shown in Figure 7. Note that the wave length λ, wave frequency f and wave velocity u_{wave} are related as $u_{wave} = \lambda f$. The wave length for the base case is L^*=25.6 mm, which gives two waves, having a wave length is $L^*/2$=12.8 mm. The base case wave length was both increased in steps to $L/L^* = 2$ and larger, and decreased to smaller values up to zero. For L/L^* above 1 the dominant wave length is between 9.6 and 12.8 mm. For L/L^* between 0.5 and 1 the dominant wave length is between 12.2 and 12.8 mm. For L/L^* below 0.5 the wave length is equal to the length of computational domain, until the waves disappear when the L/L^* falls below about 0.1. For wave lengths larger than L/L^*=0.5, the wave frequency and the wave velocity are almost independent of the length of the computation domain. As shown in Figure 8, this is also true for the resulting pressure drop and holdup ratio. When the waves disappear at small length of the computational domain, obviously the 1D values for the pressure drop and holdup ratio are retained (as presented in detail in Li et al., 2021).

Summary of findings in this section:

- The predicted wave length, wave velocity, and wave frequency are almost independent of the length of the computational domain.
- Also, predictions of pressure drop and water cut (for given total flow rate and water holdup fraction) are almost independent of the section length.

5. Two-phase versus single-phase results

To better examine what happens close to the wavy oil-water interface we also made a comparison between two-phase simulations for the oil-water flow and single-phase simulations for the water annulus. Again the base case conditions were used. The imposed total flow rate is 0.00043 m^3/s (mixture velocity of 1.24 m/s) and the imposed water holdup fraction is 0.2573 (this will give a watercut of about 20%). The water-based Reynolds number is Re_w=39000. The shear-based Reynolds is about Re_τ =140, which has a fully turbulent water annulus. First the relation between the two-phase and single-phase simulations will be demonstrated. Thereafter the single-phase approach will be used to determine the dependence of the interfacial stress on various parameters.

The two-phase simulations have shown that an almost single frequency wave is found at the interface that moves with an almost constant velocity. Therefore, observed from a reference frame that moves with that wave velocity one will see an (almost) steady flow. If so, it makes sense to change the simulation from an approach with a "fixed wall" as the frame of reference, to one in which there is a "moving wall" having an imposed velocity that is about equal to the velocity of the interfacial wave though in opposite direction. Mesh refinement was carried out for the moving wall approach for the 2D base case configuration, similarly as was done for a fixed wall as reported previously (Li et al. 2021). On the finest grid (400 points in radial direction and 200 points in streamwise direction using a domain with 12.8 mm length), there is good agreement for key output parameters like pressure drop (both give 748 Pa/m), holdup ratio h (1.21 for fixed wall versus 1.22 for moving wall) and wave amplitude A (0.73 mm for fixed wall versus 0.74 mm for moving wall). As shown in Figure 9, on the considered relatively fine numerical grid, there is only a limited deviation for interface radius and turbulent viscosity; the maximum of the ratio of the turbulent viscosity and the kinematic water viscosity (taken over the full x, r domain) is 18.8 for the fixed wall approach versus 22.5 for the moving wall approach. The conclusion is that (as expected) both approaches converge to the same solution upon grid refinement. The moving wall approach has the advantage, in comparison to the fixed wall approach, that grid convergence is faster and the required numerical time step can be larger (due to a smaller value of the maximum Courant number).

The single-phase simulations for the water annulus apply the configuration as depicted in Figure 10. The pipe section has the length λ of a single interfacial wave. The wavy interface is fixed and the straight wall of the pipe moves with an imposed (negative) velocity as indicated in the figure. The inflow and outflow velocity profiles are equal, as periodic boundary conditions are imposed. Pressure drop is handled as a source term in the momentum equation. It is important to note that the numerical method is set up such that the relative water flow rate is varied for each time step until the overall streamwise force balance (22) is satisfied. Thus the pressure drop source satisfies: $-dp/dx = 2\tau_W/R$ (where R is the pipe radius). The obtained water flow rate can be converted to a watercut by assuming a total flow rate (i.e. oil plus water) of 0.00043 m^3/s (or a mixture velocity of 1.24 m/s), which is the same total flow rate as applied in the two-phase simulation.

Figure 10 also indicates the averaged water annulus thickness d_w and the wave amplitude A. The imposed interface used has either a pure sinusoidal shape or the shape as obtained from the two-phase simulation. Obviously, a clear difference between the two approaches is that the interface in the single-phase simulation is non-deforming (with no slip boundary conditions) and the interface in the two-phase simulation is flexible. In fact the single-phase approach assumes a solid wavy oil core (or oil with an infinitely large viscosity). Furthermore there can be a pressure change across the curved interface due to oil-water interfacial tension in the two-phase approach, which does not play a role in the single-phase approach.

For the base case conditions, the following simulation approaches were compared: (1) two-phase flow, (2) single-phase water flow in the annulus with a sinusoidal interface with an amplitude that is equal to the one obtained in the two-phase simulation, and (3) single-phase water flow in the annulus with an interface that has the same shape as obtained in the two-phase simulation. The imposed velocity at the moving wall in the single-phase simulations is 1.24 m/s (which is the wave velocity obtained in the two-phase simulation), and the imposed water holdup

Figure 6. Example result showing the preferred wave length when the streamwise length of the considered pipe section is increased.

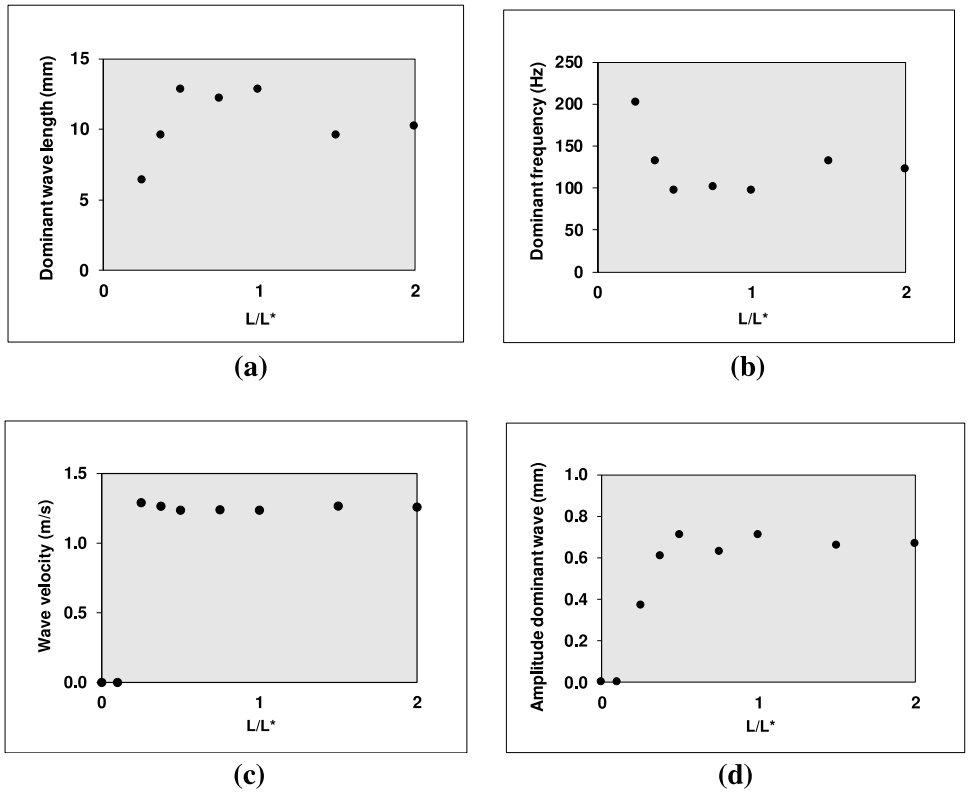

Figure 7. Dependence of the dominant wave development on the considered pipe section length L/L* (with L*=25.6 mm); (a) wave length, (b) wave frequency, (c) wave velocity, (d) wave amplitude.

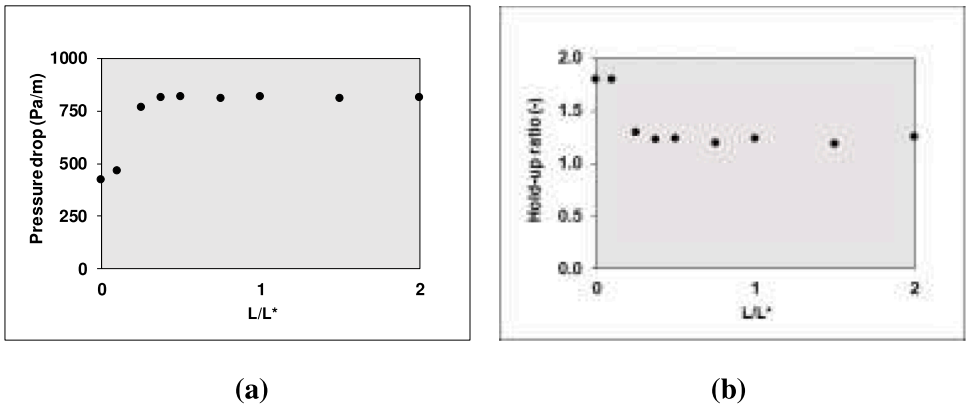

Figure 8. Pressure drop and holdup ratio for different lengths of the computational domain (using a fixed imposed value of 0.00043 m^3/s for total flow rate and of 0.2573 for water holdup fraction).

fraction is 0.2573. For all three approaches the number of grid cells was successfully refined (up to 200 cells in streamwise direction and 400 cells in radial direction) to verify that a good numerical accuracy was obtained.

The numerical values of selected output parameters are compared in Table 2. Pressure drops are quite close, albeit that the value for the single-phase simulation with sinusoidal interface is 12% lower than for the other two. The watercut found in the single-phase simulation with sinusoidal interface is slightly lower than the value found in the two-phase simulation, and it also has a higher value of the holdup ratio; the agreement with the two-phase result is better for the single-phase simulation with imposed two-phase interface. The table also shows values (averaged along streamwise direction) for the wall shear stress and for the interfacial stress. The latter is also splitted in a pressure contribution and in a viscous stress (or shear stress) contribution. The pressure contribution at the interface can be found from integration of pressure along the location of the interface in streamwise direction. This pressure contribution can also be described as “form drag”, and its percentage contribution to the total interfacial stress is included in the table as well. Obviously, form drag will be zero in absence of waves, but for the considered conditions most of the interfacial stress is due to form drag.

Some quantities as obtained with the three modelling approaches are compared in Figure 11, which shows the interface shape, maximum turbulent viscosity, interface pressure and interface shear stress. When the two-phase interface is compared with the sinusoidal interface (Figure 11a), the two-phase result shows the typical saw-tooth shape. Predictions for the turbulent viscosity in the three approaches (Figure 11b) are quite close. There is also good agreement for the interface pressure (Figure 11c) although the peak in the single-phase

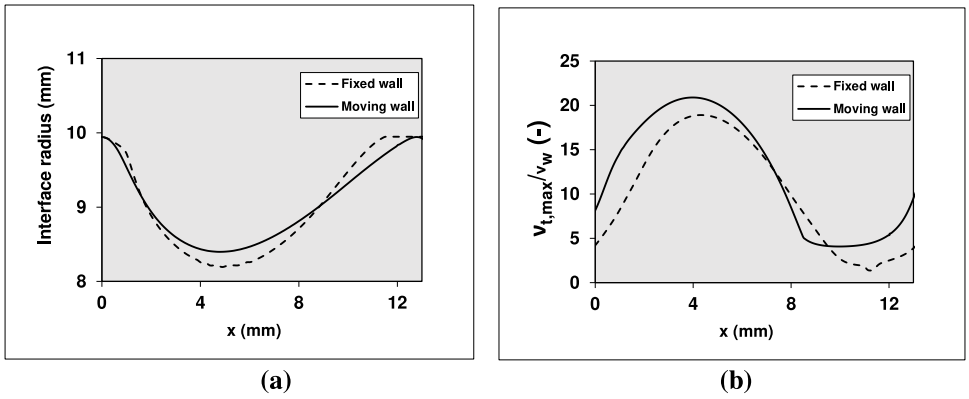

Figure 9. Fixed wall approach versus moving wall approach for the 2D base case configuration using 200 points in streamwise direction and 400 points in radial direction; (a) interface location, (b) maximum turbulent viscosity.

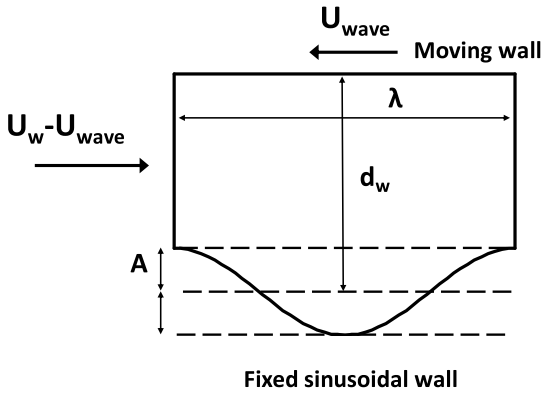

Figure 10. Configuration for single-phase simulations.

simulation with sinusoidal interface is slightly shifted, which is in line with the difference in interface shape.

As shown by the shear stress at the interface in Figure 11d, which includes zero crossings, there is a water recirculation zone along the wave interface. The shear stress for the two-phase simulation is omitted from the graph, as it is difficult to accurately deduce that profile from the simulation results. The recirculation zone is more clearly illustrated in Figure 12, which shows the streamlines. To understand the physics, one should realize that the bulk flow of water, when travelling with the wave, moves from right to left in the figure. The increasing annulus thickness (from right to left) causes the water layer to separate from the interface. In downstream direction (seen from the bulk water moving from right to left), where the thickness of the annulus converges again, the water layer reattaches, which closes the recirculation zone.

Impingement of the bulk water layer on the interface at the reattachment location causes a pressure peak (see Figure 11c) that gives a main contribution to the form drag (Table 2). Flow in the recirculation gives a shear stress contribution that is opposite to the direction of the pressure stress (form drag).

Summary of findings in this section:

- Simulations with either a fixed frame of reference or with a moving-wall frame of reference give similar results.
- The single-phase simulation with sinusoidal interface gives a good agreement with the two-phase approach.
- Therefore the single phase model with imposed waviness can be used to study the effect of wave structure on the annulus flow,

6. Concentric single-phase results

In the previous section it was found that the single-phase simulation with sinusoidal interface gives a good agreement with the two-phase approach. Therefore, it is attractive to use the single-phase approach for a sensitivity study. We are particularly interested in the dependence of pressure drop and water holdup on the wave structure at the interface. The single-phase approach allows to carry out such a sensitivity assessment relatively quickly (i.e. at relatively low computational cost).

Single-phase simulations were carried out for the base case configuration, in which the wave length was varied as 25.6, 12.8, and 6.4 mm, and the wave amplitude was varied between zero and about 1 mm. A

Table 2
Comparison of single-phase and two-phase simulations for the base case conditions (using a fine 200×400 mesh).

Quantity	Unit	Twophase	Single phase sinusoidal interface	Single phase interface same as twophase
Pressure drop	Pa/m	748	657	760
Watercut	%	22.1	20.0	21.4
Holdup ratio (h)		1.22	1.39	1.27
Wall shear stress	Pa	3.9	3.4	4.0
Total interface stress	Pa	3.4	3.0	3.4
Interface pressure stress	Pa	2.5	2.5	3.4
Interface viscous stress	Pa	0.9	0.5	0.0
Form drag at interface	%	73	84	100

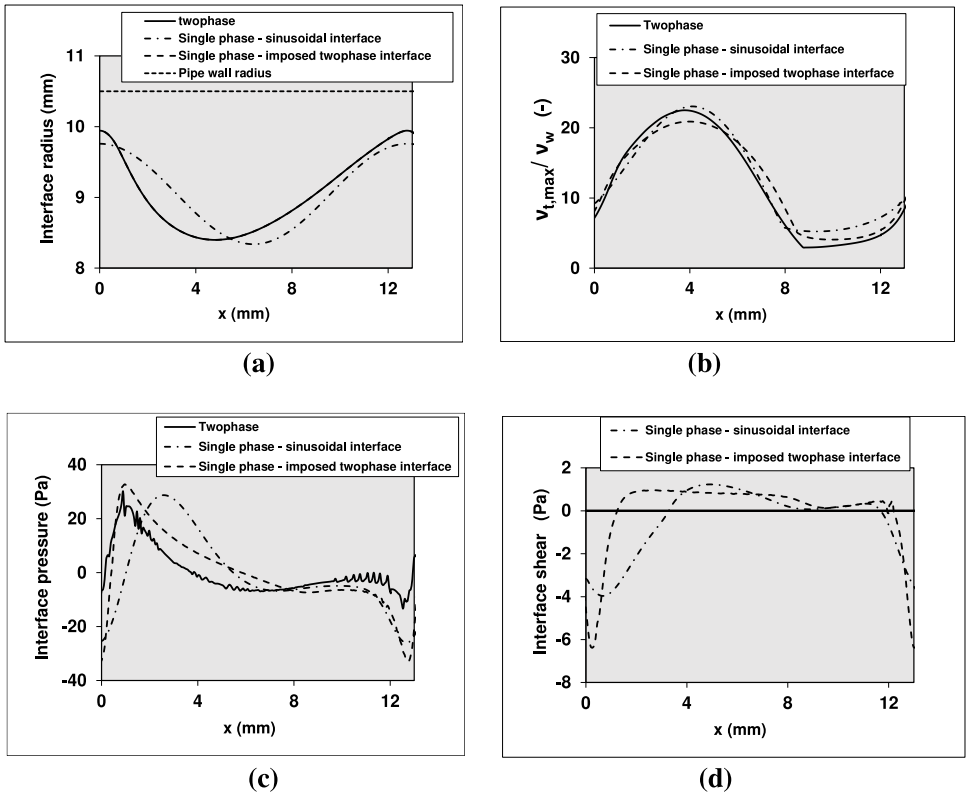

Figure 11. Comparison of single-phase and two-phase simulations for the base case conditions (using a fine 200×400 mesh); (a) interface location, (b) maximum turbulent viscosity, (c) interface pressure, (d) interfacial shear stress.

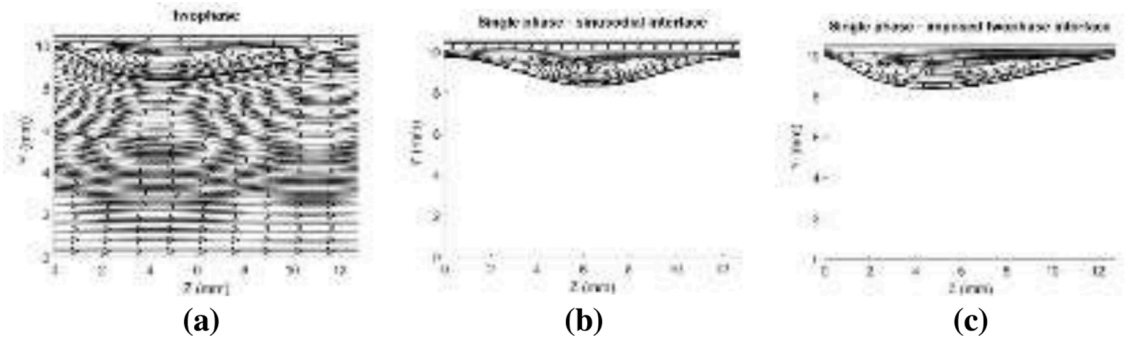

Figure 12. Streamlines showing recirculation zone for single-phase and two-phase simulation for the base case conditions; (a) two-phase, (b) single-phase with sinusoidal interface, (c) single-phase with imposed two-phase interface.

pure sinusoidal interface was prescribed in the moving wall simulations (see Figure 10). As explained before, the resulting water flow rate in each simulation is such that the overall force balance for the pipe is satisfied with $-dp/dx = \frac{2\tau_w}{R}$ (being eq. 22). To make a meaningful comparison, the watercut was fixed at 20% (based on a total flow rate, i.e. oil plus water) of 0.0043 m^3/s, or a mixture velocity of 1.24 m/s). This requires to properly take the (implicit) presence of oil flow in the core into account. This is done by using eq. (25) for the interface velocity, while neglecting the first term on the right hand side of the equation (which indeed can be verified to be very small for large values of the oil/water viscosity ratio). Basically this means that the oil core is predicted by a velocity profile that is everywhere equal to the average oil velocity, and also the interfacial wave velocity is equal to the average oil velocity. This all means that as part of the numerical iteration process, the water holdup fraction (i.e. the average interface location) has to be determined such that the 20% watercut is found. Note that the 20% watercut for a total flow rate of 0.00043 m^3/s corresponds to a water flow rate of 8.6×10^{-5} m^3/s.

The single-phase simulation results for the pressure drop, water holdup fraction and maximum turbulent viscosity are shown in Figure 13. The concentric two-phase simulation results are also included, which are in good agreement with the single-phase predictions for a wave length of 12.8 mm. For amplitudes above about 0.9 mm, the water annulus becomes locally so thin that the turbulent viscosity drops due to relaminarization. For amplitudes between about 0.6 mm and 0.9 mm the pressure drop reaches a maximum plateau level. The smallest considered wave length of 6.4 mm gives the lowest turbulence levels and herewith the lowest pressure drop.

The increase in pressure drop (up to a plateau value) for increasing amplitude of the interfacial waves, with fixed total flow rate can be explained as follows. A larger wave amplitude gives an increased grip of the oil flow on the water flow. The increased interfacial stress gives an increased water bulk velocity (at fixed total flow rate with fixed watercut) in a thinner water annulus. The increased water bulk velocity

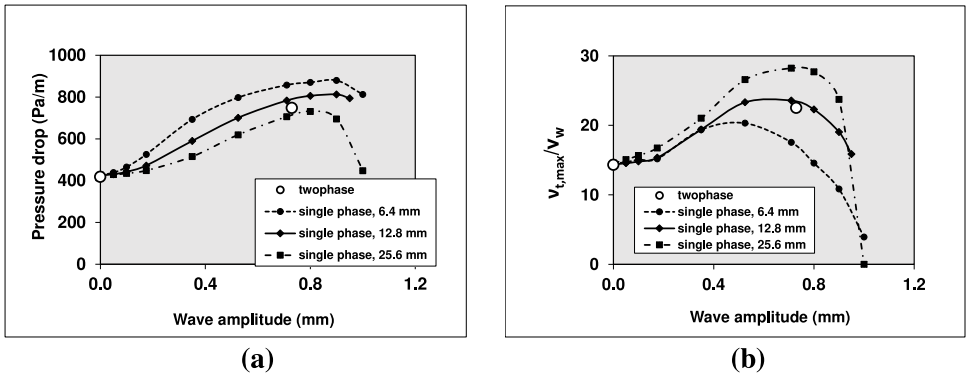

Figure 13. Single-phase simulations for the water annulus with sinusoidal wavy interface for the base case configuration with 20% watercut; dependence on wave amplitude of (a) pressure drop, (b) maximum turbulent viscosity.

gives a higher wall shear stress, and herewith a higher pressure drop.

The dimensionless pressure drop (being the Fanning friction factor at the wall) and the water hold-up / watercut dependence (being the holdup fraction) are shown in Figure 14. The figure also includes the value for the friction factor for single-phase water flow; if the wave amplitude is sufficiently large (say between 0.6 mm and 0.9 mm) the friction factor for the core-annular flow is close to the water-only value. This is consistent with the reduced value of the holdup ratio for these relatively large values of the wave amplitude, where the large interfacial stress has reduced the water accumulation tendency.

Figure 15a shows the interfacial friction factor f_i, which is defined through $\tau_i = f_i \frac{1}{2}\rho_w(u_i - u_w)^2$. Here u_i is interface velocity and u_w is the bulk water velocity.

The interfacial friction is built up of a shear stress part and a form stress part, i.e. $f_i = f_{shear} + f_{form}$. Figure 15b shows the dependence of the ratio f_{form}/f_i on wave amplitude: the form drag becomes dominant at about 90% of the interfacial stress if the wave amplitude increases to about 0.9 mm in the base case configuration.

It is also attractive to apply the single-phase approach to determine the effect of watercut on the core-annular flow behaviour. Again the same procedure as described above was followed, albeit now for different watercuts. The prescribed total flow rate in the base case configuration is 0.00043 m^3/s, corresponding to a mixture velocity of 1.24 m/s. Results for the pressure drop and for the maximum turbulent viscosity, with various values of the wave amplitude, as simulated with the 2D model (i.e. concentric flow, without gravity) are shown in Figure 16. In fact the results for zero wave amplitude were obtained with the 1D two-phase model (see Li et al., 2021). The single-phase results with non-zero amplitude waves and the 1D two-phase results (i.e. zero wave amplitude) also compared with the 2D two-phase results. If the wave amplitude is sufficiently high (i.e. say above 0.35 mm), giving sufficient interfacial stress, the pressure drop will become very close to the water only case (at the same fixed total flow rate). When for a given wave height, the watercut is increased to almost 100%, results for pressure drop and maximum turbulent viscosity will show a jump when the oil core becomes very small. This is because there is a discontinuity in the configuration: from one with a thin wave core to one where the core is totally absent. Though the jump in the values is not very large here.

The results can also be made dimensionless by using the following two important quantities: the Fanning wall friction factor f_W and the holdup ratio h. As shown in Figure 17, trends are as expected: an increasing wave amplitude gives an increasing friction factor (more wall friction) and a decreasing holdup ratio (less apparent slip between the water and oil flows). The friction factor and holdup ratio are not very strongly dependent on watercut. The wave amplitude in the two-phase results increases with increasing watercut. The two-phase results for the friction factor, like the single-phase results for the larger wave amplitudes, are almost independent of watercut. The holdup ratio gradually decreases with increasing watercut.

Figures 16 and 17 also include the "water equivalent" RANS results, as a function of the (apparent) watercut fraction. These water equivalent results are found from the simulation for water-only flow in the pipe; in the interpretation of these results, they are "artificially" splitted in a core and annulus (while these two thus have the same properties for the viscosity and density); see also section 8. The pressure drop is 750 Pa/m and the Fanning friction factor is 0.0052. The two-phase water-oil results for the holdup ratio are close to the water-equivalent results (giving h =1.2 for large watercut). The maximum turbulent viscosity for the two-phase results is lower than for the water-equivalent results. This shows that the presence of the oil core mitigates turbulence in the water annulus.

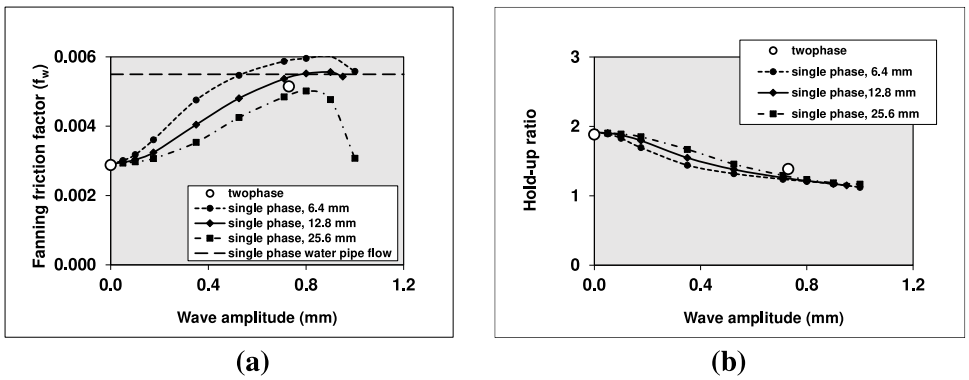

Figure 14. Single-phase simulations for the water annulus with sinusoidal wavy interface for the base case configuration with 20% watercut; dependence on wave amplitude for (a) Fanning friction factor at the wall, (b) holdup ratio.

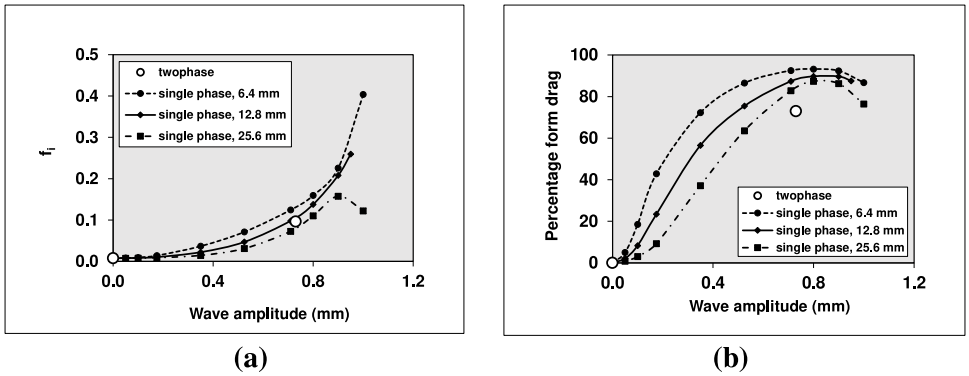

Figure 15. Single-phase simulations for the water annulus with sinusoidal wavy interface for the base case configuration with 20% watercut; dependence on wave amplitude for (a) interface friction factor, (b) from drag contribution to interfacial stress.

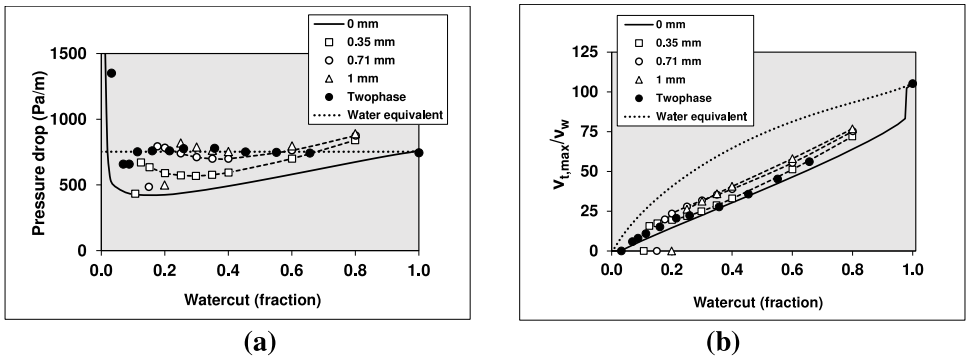

Figure 16. Single-phase simulations for the water annulus with sinusoidal wavy interface for the base case configuration with fixed total flow rate; dependence on watercut for (a) pressure drop, (b) maximum turbulent viscosity.

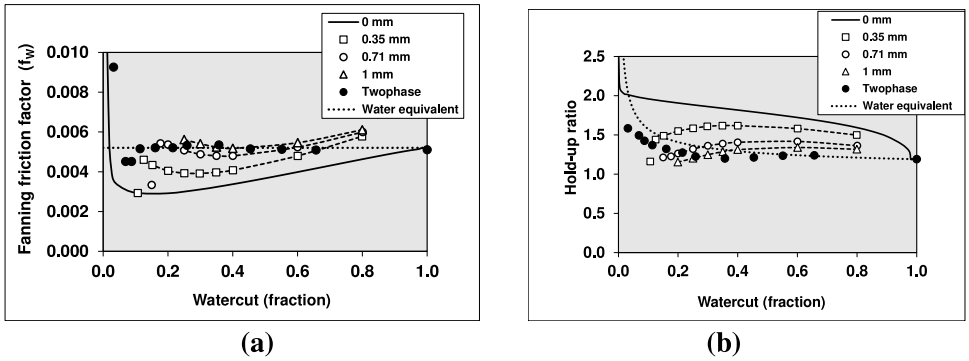

Figure 17. Single-phase simulations for the water annulus with sinusoidal wavy interface for the base case configuration with fixed total flow rate; dependence on watercut for (a) Fanning friction factor, (b) hold-up ratio.

Figures 16 and 17 also show that the two-phase prediction (with fixed total flow rate) has a minimum in the pressure drop (and also in the Fanning friction factor for the wall) when the watercut is decreased. This is due to the relaminarization of the water annulus. For very low watercut, the pressure drop (and also the Fanning friction factor) increases again. This is because now the (high viscous) oil core is so close to the wall that it imposes a high stress on the water annulus and herewith on the pipe wall, even though the flow is laminar. The minimum and the sharp increase for pressure drop and Fanning friction factor at decreasing watercut is also clearly visible in the simulations without interfacial waves (zero wave amplitude).

Summary of findings in this section:

- The integral force balance for core annular flow includes the wall friction between the water annulus and the pipe wall and the interfacial stress between the oil core and the water annulus. The interfacial stress depends on length and amplitude of the waves at the interface.
- The wall friction and interfacial stress can be determined from the RANS simulations.
- Unless the waves are absent or the imposed wave amplitude is very small, travelling waves easily create sufficient stress on the water annulus, such that it is apparently felt by the pipe wall as a fully turbulent single-phase water flow.
- Most of the interfacial stress is due to form drag (with local water recirculation zones with respect to an observer travelling with the waves) and only a small part is due to shear stress.

- The water hold-up fraction for core-annular flow closely agrees with the value found for the so-called "water equivalent flow" (i.e. single phase water pipe flow, with an artificial split between a water core and a water annulus).
- A good estimate of the frictional pressure drop and holdup ratio of core annular flow with a turbulent water annulus is to take the Fanning friction factor the same as the well-known value for water only pipe flow and the holdup ratio the same as for the equivalent water flow (i.e. about h =1.2).

7. Eccentric single-phase results

The single-phase RANS model was also used to investigate the effect of an eccentric core. Thereto again the base case configuration was considered (as defined in section 2.3). The total flow rates was fixed at 0.00043 m^3/s, or a mixture velocity of 1.24 m/s, with 20% watercut. The interface has either no waves or waves with a prescribed amplitude of 0.71 mm. The pipe section length was set to 12.8 mm.

To create an eccentric case in the single-phase simulation for the annulus, the imposed interface with waves was moved in the direction to the top of pipe. If the (average) water layer thickness at the top and bottom are denoted as d_{top} and d_{bottom}, respectively, the eccentricity is defined as $e = \frac{d_{bottom}-d_{top}}{d_{bottom}+d_{top}}$. Thus $e = 0$ for a concentric oil core, and $e = 1$ for a fully eccentric oil core. An eccentric core requires carrying out a 2D single-phase simulation when there are no waves (i.e. no 3D simulation is needed as the flow is the same in each cross sectional plane) and a 3D single-phase simulation when there is a finite-amplitude wave. The simulation results for pressure drop and maximum turbulent viscosity are shown in Figure 18, and for Fanning friction factor at the wall and holdup ratio in Figure 19. As the top/bottom water annulus becomes thinner/thicker with increasing eccentricity, the turbulence level increases in the bottom layer and decreases in the top layer. If the eccentricity becomes too high the top water annulus relaminarizes. The effect of eccentricity on pressure drop, friction factor, and holdup ratio is small.

Assuming a horizontal pipe with gravity, Figure 20 shows the pressure force (corrected for water hydrostatic head) and the shear force on the oil core in vertical direction. These forces are scaled with the buoyancy force (which is known from the holp-up fraction and from water and oil densities specified in section 2.3). This shows that the eccentricity (i.e. oil core located in the direction of the pipe top) gives both downward directed pressure and shear forces. In this example, there is a force equilibrium at an eccentricity of about e=0.19. In the absence of waves the vertical pressure force (corrected for water hydrostatic head) is zero (as there is parallel flow), whereas the downward shear force turns out to be very small (being insufficient to compensate the buoyancy force). This thus confirms that waves are needed to prevent the oil core from touching the upper wall in horizontal core-annular flow.

Summary of findings in this section:

- The dimensionless pressure drop (which is the Fanning friction factor for the wall) is almost independent of eccentricity, and equal to the water-only value.
- There is also an eccentricity where the vertical force balance for the single phase annulus simulation is satisfied, with a downward directed pressure force and a downward directed shear force.
- Such a balance cannot be found in the RANS results for eccentric core-annular flow without interface waves. This supports the conjecture that waves are needed to enable stable horizontal core-annular flow.

8. Comparison with experiments and DNS

Figure 21 compares the concentric, two-phase RANS simulations with experiments by Van Duin et al., 2019) and by Sotgia et al. (2008). The "friction factor ratio" is shown, which is defined as the ratio of the Fanning friction factor at the given watercut and the Fanning friction factor for water only flow. In the sections above we have argued that the pressure drop for two-phase core annular flow is about the same as found for water only flow (at the same total flow rate) for all watercuts, except for low values. This is confirmed by the comparison in Figure 21.

The single phase simulation for the water annulus in a horizontal pipe for the base case conditions at eccentricity e=0.19 (which satisfies the vertical force balance as shown in section 7) is compared with the water-oil interface obtained in experiments by Duin et al. (2017). There is very good agreement; the experiment has only a slightly lower eccentricity of e=0.12. In fact, for both the single phase simulation and the experiment the eccentricity is very small (see also Figure 21). This is in contrast to the (eccentric) 3D two-phase simulation result, as presented in our earlier study (Haoyu et al., 2021), which gives a much larger eccentricity (e=0.7) than the experiment. This is probably due to laminarization in the RANS model for the top water annulus, compared to a fully turbulent bottom layer. Work is ongoing to further investigate this (using the type of approach with single phase simulations and performing a vertical force balance as outlined in the present paper).

As accurate experimental results for the holdup ratio as a function of the watercut for core-annular flow seem to be missing in the literature, we have used the Direct Numerical Simulation results by Kim & Choi (2018) as a reference for validation of the RANS model and the different mechanistic models. They simulated 5 watercut conditions for the pipe flow that were also used in the experiments by Vanegas Prada (1999); see Table 1. The simulation results for the Fanning friction factor (f_W), the friction factor ratio, and the holdup ratio (h) for the five watercut conditions are shown in Figure 23. All simulations (i.e. RANS and DNS) have a fixed prescribed frictional pressure drop of 400 Pa/m.

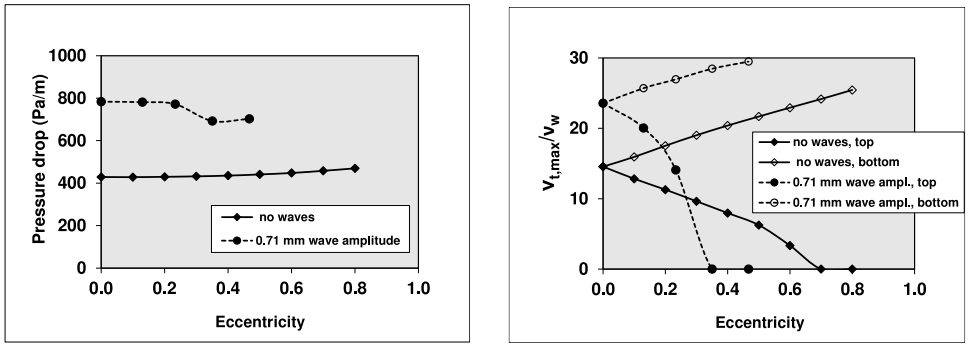

Figure 18. Single-phase simulations for the water annulus with sinusoidal wavy interface for the base case configuration with 20% watercut; dependence on eccentricity for (a) pressure drop, (b) maximum turbulent viscosity.

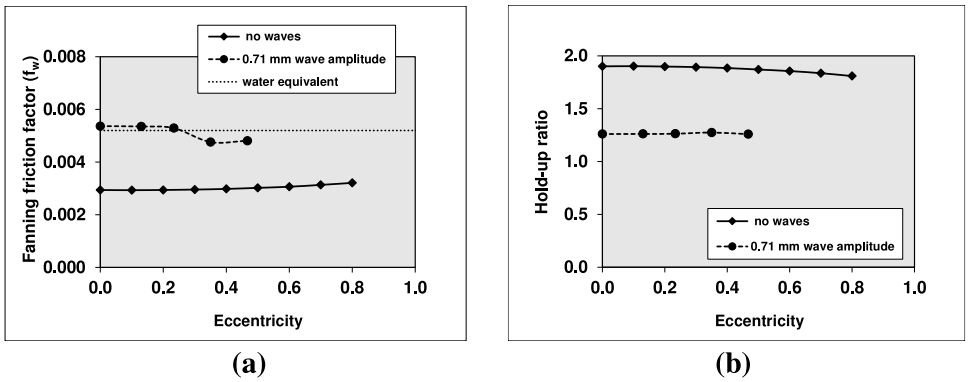

Figure 19. Single-phase simulations for the water annulus with sinusoidal wavy interface for the base case configuration with 20% watercut; dependence on eccentricity for (a) Fanning friction factor at the wall, (b) holdup ratio.

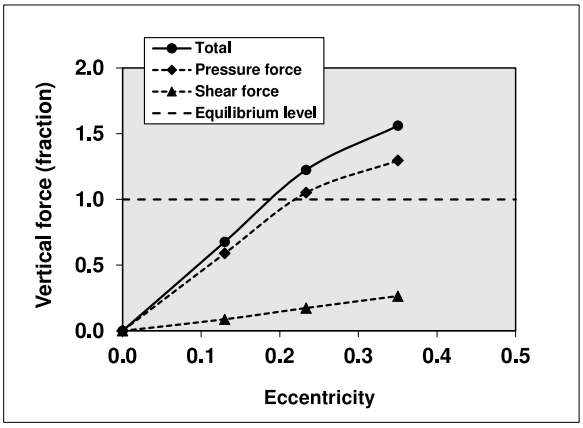

Figure 20. Single-phase 3D simulations for the water annulus with sinusoidal wavy interface with 0.71 mm amplitude for the base case configuration with 20% watercut; vertical forces on the oil core.

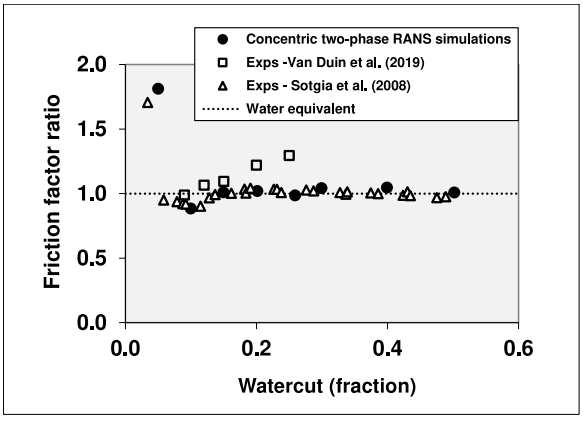

Figure 21. Comparison between simulations and experiments; Fanning friction factor versus watercut.

For all 5 watercuts, except for the smallest value, for which DNS results are available, the Fanning friction factor is almost the same as for turbulent flow with only water (i.e. all oil is assumed to be replaced been replaced by water). As shown in Figure 23a, the lowest watercut in DNS gives a higher value for the Fanning friction factor, which is because now the water annulus is so thin that is gives laminar flow instead of turbulent flow. Considering the 4 watercuts with turbulent water annulus, the Fanning friction factor that is found from our RANS

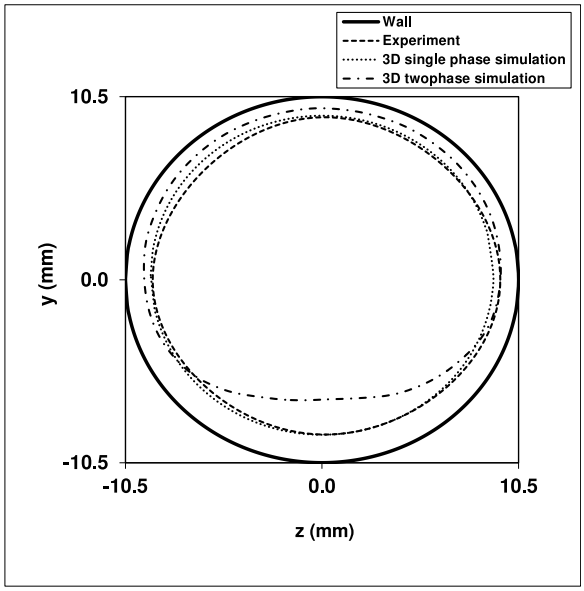

Figure 22. Comparison between simulations and experiments; Average location of the water-oil interface.

simulations is also almost independent of watercut, but it is about 18% smaller than the DNS results, 17% smaller than the single-phase water value found with the Churchill correlation, and 11% smaller than the single-phase water value found with Launder & Sharma $k-\varepsilon$ model. As the Churchill correlation for the Fanning friction factor is almost exact for single-phase water flow, this also shows that the Launder & Sharma $k-\varepsilon$ model underpredicts single-phase turbulent pipe flow by (17-11=) 6%. For the 4 watercuts with turbulent annulus, the Ullmann & Brauner model prediction for the Fanning friction factor is only about 3% higher than DNS predictions.

The DNS and RANS predictions for the holdup ratio h are compared in Figure 23c. Also included are expressions used by Oliemans, Bai et al., and Ullmann & Brauner (as referred to in section 3). The DNS and RANS results show a slow decrease of the holdup ratio for increasing watercut; this means that the water accumulation effect (i.e. WC $>\alpha_w$) decreases when the watercut becomes larger. For the 4 watercut values used in the DNS (with turbulent water annulus) the RANS prediction for the holdup ratio is about 12% above the DNS prediction. Thus the water accumulation effect is larger in RANS than in DNS.

Figure 23c also includes a curve denoted as the "water equivalent" holdup ratio. As already mentioned in section 6, this curve is found by considering water-only flow, that is "artificially" splitted in a core and annulus (while they still have same properties for viscosity and density).

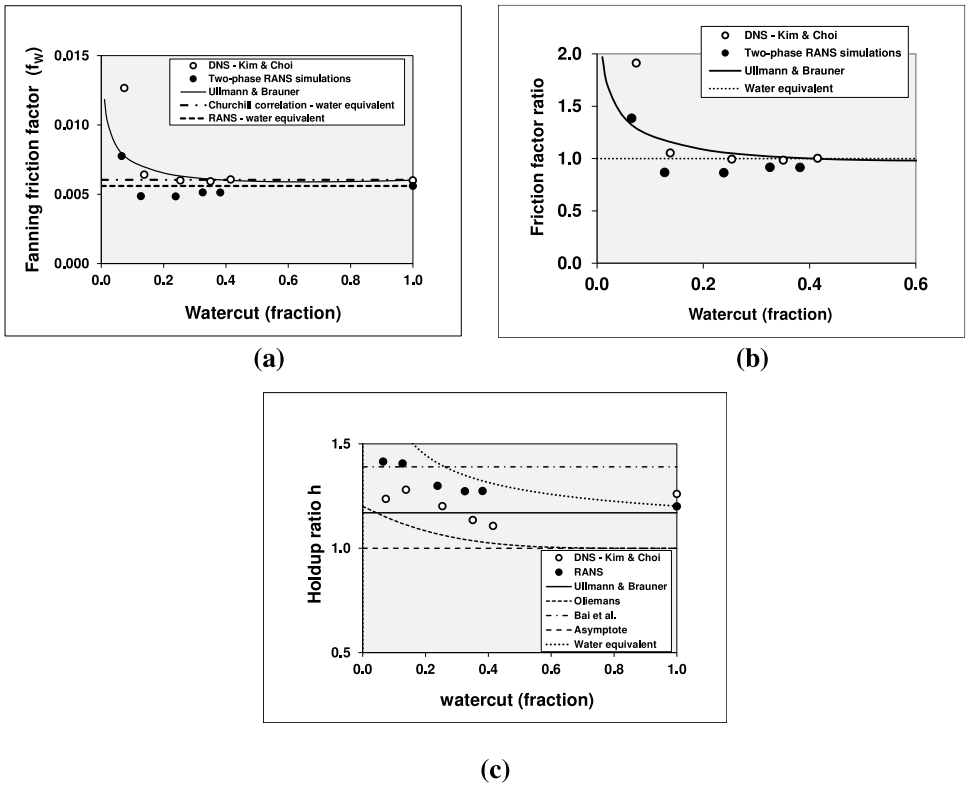

Figure 23. Comparison of RANS and mechanistic models (or correlations) with DNS results for different watercuts by Kim & Choi (2018) at a fixed frictional pressure drop is 400 Pa/m; (a) Fanning friction factor, (b) Friction factor ratio, (c) hold-up ratio.

The watercut and holdup ratio are now referring to the annulus part of the single-phase RANS results; here the watercut is determined by integrating the RANS velocity profile in the annulus to give the water flow rate in the annulus, and divide this by the total flow rate through the pipe. This shows that there is relatively much water accumulation close to the pipe wall for low watercut, where water is slowed down due to the wall presence. For high watercut (i.e. vanishing core layer) the holdup ratio decreases to $h = u_{centre}/u_{bulk}$ (i.e. the ratio of water velocity at the pipe centre and average water velocity over the pipe cross section). It is helpful to be aware of this natural accumulation effect when interpreting the holdup ratio for core-annular flow with a real difference in viscosity between the core liquid and the annulus liquid. In fact this means that the increase in holdup ratio found for decreasing watercut in the DNS and RANS for the configuration of Kim & Choi can (at least) partly be explained from this natural accumulation effect.

The largest three watercuts have a shear-based Reynolds number as Re_τ that is above 90, which gives a turbulent water annulus. The lowest watercut of 7% has $Re_\tau = 33$, which gives a laminar water annulus. A more detailed comparison of the RANS and DNS simulation results is in preparation, and will appear as a separate paper.

Summary of findings in this section:

- The simulation results were validated by comparison with different sets of experimental data (particularly with those by Sotgia et al. and by Duin et al.) and with the Direct Numerical Simulations by Kim & Choi. The comparison supports the theoretical findings.
- More work is needed to understand the effect of gravity in horizontal core-annular flow (through different types of models, e.g. RANS, LES, DNS, and experiments).

9. Conclusions

1 Simulations were carried out for core-annular flow with a turbulent water annulus through solving the RANS two-phase equations with the Launder-Sharma low-Reynolds number $k-\varepsilon$ model. The flow is characterized by travelling waves at the oil-water interface. As expected, the simulations with either a fixed frame of reference or with a moving-wall frame of reference give similar results.

2 Unless the pipe section length in the simulation is chosen too short, the predicted wave length, wave velocity, and wave frequency are almost independent of the length of the computational domain. Also the predictions of the pressure drop and water cut (for given total flow rate and water holdup fraction) are almost independent of the section length.

3 A review of different sets of lab data for core-annular flow shows that the Fanning friction factor for the wall, which makes the pressure drop dimensionless with the dynamic pressure based on water density and mixture velocity, is an attractive parameter. In the experiments, that friction factor is close to the value found for turbulent water-only flow, and almost independent of watercut.

4 A force balance for core annular flow was considered, which includes the wall friction between water annulus and pipe wall and the interfacial stress between oil core and water annulus. The wall friction and interfacial stress were determined from the RANS simulations. The interfacial stress will be dependent on length and amplitude of the waves at the interface. Details could be simulated through considering a single phase RANS model for the water annulus with imposed waviness on a moving wall.

5 Unless the waves are absent or the imposed wave amplitude is very small, travelling waves easily create sufficient stress on the water annulus, such that it is apparently felt by the pipe wall as a fully turbulent single-phase water flow. Most of the interfacial stress is due to form drag (with local water recirculation zones with respect to an observer travelling with the waves) and only a small part is due to shear stress.

6 The water hold-up fraction for core-annular flow, which is a second important quantity next to the Fanning wall friction

factor, closely agrees with the value found for the so-called "water equivalent flow" (i.e. single phase water pipe flow, with an artificial split between a water core and a water annulus).

7 A good estimate of the frictional pressure drop and holdup ratio of core annular flow with a turbulent water annulus is to take the Fanning friction factor the same as the well-known value for water only pipe flow and the holdup ratio the same as for the equivalent water flow (giving about $h = 1.2$).

8 By re-writing the mechanistic model of Ullmann & Brauner, we found that this estimate is actually also hidden in that model. The RANS simulation show that a different behaviour is only found when the watercut is decreased to a very low value, where the water annulus becomes so thin that it relaminarizes. Here the near-wall presence of the moving oil core with the high imposed shear determines the wall friction.

9 Simulations were also carried out with the single phase RANS model for the water annulus for an eccentric rather than a concentric interface for horizontal pipe flow. Again, the dimensionless pressure drop (which is the Fanning friction factor for the wall) is almost independent of the eccentricity, and equal to the water-only value. There is also an eccentricity where the vertical force balance for the single phase annulus simulation is satisfied, with a downward directed pressure force and a downward directed shear force. These two forces balance the upward buoyancy force, and they physically make up the levitation mechanism that prevent that the oil core touches the top wall. Such a balance cannot be found in the RANS results for eccentric core-annular flow without interface waves. This supports the conjecture that waves are needed to enable stable horizontal core-annular flow.

10 The simulation results were validated by comparison with different sets of experimental data (particularly with those by Sotgia et al. and by Duin et al.) and with Direct Numerical Simulations by Kim & Choi. The comparison supports the theoretical findings.

Declaration of Competing Interest

All authors have participated in (a) conception and design, or analysis and interpretation of the data; (b) drafting the article or revising it critically for important intellectual content; and (c) approval of the final version.

This manuscript has not been submitted to, nor is under review at, another journal or other publishing venue.

The authors have no affiliation with any organization with a direct or indirect financial interest in the subject matter discussed in the manuscript.

Acknowledgement

The first author has received a grant from the China Scholarship Council (CSC). Thanks are also due the Netherlands Foundation of Scientific Research (NWO) for supplying the computer time.

References

Arney, M.S., Bai, R., Guevara, E., Joseph, D.D, Liu, K., 1993. Friction factor and holdup studies for lubricated pipelining-I. Experiments and correlations. Int. J. Multiphase Flow 19, 1061–1076.

Bai, R., Chen, K., Joseph, D.D., 1992. Lubricated pipelining: stability of core-annular flow. part 5. experiments and comparison with theory. J. Fluid Mechanics 240, 97–132.

Bai, R., Kelkar, K., Joseph, D.D., 1996. Direct simulation of interfacial waves in a high-viscosity-ratio and axisymmetric core-annular flow. Journal of Fluid Mechanics 327, 1–34.

Bannwart, A.A., 2001. Modeling aspects of oil-water core-annular flows. J. Petrol. Sci. Engng 32, 127–143.

Beerens, J.C., Ooms, G., Pourquié, M.J.B.M., Westerweel, J., 2014. A comparison between numerical predictions and theoretical and experimental results for laminar core-annular flow. AIChE Journal 60 (8), 3046–3056.

Chen, K., Bai, R., Joseph, D.D., 1990. Lubricated pipelining. Part 3 Stability of core-annular flow in vertical pipes. Journal of Fluid Mechanics 214, 251–286.

Ghosh, S., Mandal, T.K., Das, P.K., 2009. Review of oil water core annular flow. Renewable and Sustainable Energy Rev 13, 1957–1965.

Grassi, B., Strazza, D., Poesio, P., 2008. Experimental validation of theoretical models in two-phase high-viscosity ratio liquid–liquid flows in horizontal and slightly inclined pipes. Int. J. Multiphase Flow 34, 950–965.

Hu, H., Jing, J., Tan, J., Yeoh, G.H., 2020. Flow patterns and pressure gradient correlation for oil–water core–annular flow in horizontal pipes. Experimental and Computational Multiphase Flow 2, 99–108.

Huang, A., Christodoulou, C., Joseph, D.D., 1994. Friction factor and holdup studies for lubricated pipelining - II; laminar and k-ϵ models of eccentric core flows. Int. J. Multiphase Flow 20, 481–491.

Ingen Housz, E.M.R.M., Ooms, G., Henkes, R.A.W.M., Pourquie, M.J.B.M., Kidess, A., Radhakrishnan, R., 2017. A comparison between numerical predictions and experimental results for core-annular flow with a turbulent annulus. Int. J. Multiphase Flow 95, 271–282.

Jiménez, J., Moin, P., 1991. The minimal flow unit in near-wall turbulence. J. Fluid Mechanics 225, 213–240.

Joseph, D.D., Bai, R., Chen, K.P., Renardy, Y.Y., 1997. Core-Annular Flows. Annular Review of Fluid Mechanics 29, 65–90.

Kim, K., Choi, H., 2018. Direct numerical simulation of a turbulent core-annular flow with water-lubricated high viscosity oil in a vertical pipe. J. Fluid Mech. 849, 419–447.

Ko, T., Choi, H.G., Bai, R., Joseph, D.D., 2002. Finite element method simulation of turbulent wavy core-annular flows using a k-ω turbulence model method. Int. J. Multiphase Flow 29, 1205–1222.

Launder, B.E., Sharma, B.T., 1974. Application of the energy dissipation model of turbulence to the calculation of flow near a spinning disc. Lett. Heat and Mass Transfer 1, 131–138.

Li, H., Pourquié, M.J.B.M., Ooms, G., Henkes, R.A.W.M., 2021. Simulation of turbulent horizontal oil-water core-annular flow with a low-Reynolds number k-ϵ model. Int. J. Multiphase Flow 142, 103744.

Oliemans, R.V.A., 1986. The lubricating-film model for core-annular flow. Delft University of Technology. PhD Thesis.

Oliemans, R.V.A., Ooms, G., Wu, H.L., Duijvestein, A., 1987. Core-annular oil/water flow: the turbulent-lubricating-film model and measurements in a 5 cm pipe loop. Int. J. Multiphase Flow 13, 23–31.

Ooms, G., Pourquié, M.J.B.M., Poesio, P., 2012. Numerical study of eccentric core-annular flow. Int. Journal of Multiphase Flow 42, 74–79.

Rodriguez, O.M., Bannwart, A.C., 2006. Experimental study on interfacial waves in vertical core flow. J. Petroleum Science and Engineering 54, 140–148.

Shi, J., Lao, L., Yeung, H., 2017. Water-lubricated transport of high-viscosity oil in horizontal pipes: The water holdup and pressure gradient. Int. J. Multiphase Flow 96, 70–85.

Sotgia, G., Tartarini, P., Stalio, E., 2008. Experimental analysis of flow regimes and pressure drop reduction in oil–water mixtures. Int. J. Multiphase Flow 34, 1161–1174.

Tripathi, S., Tabor, R.F., Singh, R., Bhattacharya, A., 2017. Characterization of interfacial waves and pressure drop in horizontal oil-water core-annular flows. Physics of Fluids 29, 082109.

Ullmann, A., Brauner, N., 2004. Closure relations for the shear stress in two-fluid models for core-annular flow. Multiphase Science and Technology 16, 355–387.

Van Duin, E., Henkes, R.A.W.M., Ooms, G., 2019. Influence of oil viscosity on oil-water core-annular flow through a horizontal pipe. Petroleum 5 (2), 199–205.

Vanegas Prada, J.W., 1999. Estudo experimental do escoamento anular óleo-áqua ("core flow") na elevação de óleos ultraviscosos. University of Campinas, Brazil. Master Thesis.

Yamamoto, T., Okano, Y., Dost, S., 2017. Validation of the S-CLSVOF method with the density-scaled balanced continuum surface force model in multiphase systems coupled with thermocapillary flows. Int. J. for Numerical Methods in Fluids 83 (3), 223–244.